In-situ observations of dislocation recovery and low angle boundary formation in deformed aluminium

IOP Conf. Series: Journal of Physics: Conf. Series **1270** (2019) 012010 doi:10.1088/1742-6596/1270/1/012010

In-situ observations of dislocation recovery and low angle boundary formation in deformed aluminium

H W Ånes[1], A T J van Helvoort[2] and K Marthinsen[1]

[1]Department of Materials Science and Engineering, Norwegian University of Science and Technology, N-7491 Trondheim, Norway
[2]Department of Physics, Norwegian University of Science and Technology, N-7491 Trondheim, Norway

E-mail: hakon.w.anes@ntnu.no

Abstract. An experimental study of the recovery of dislocations and low angle boundary formation in aluminium is presented. By combining *in-situ* annealing with orientation mapping in the transmission electron microscope, maps of geometrically necessary dislocation estimates derived from orientation measurements and subgrain formation can be quantitatively analysed. A thin foil of a commercially pure aluminium alloy cold-rolled to a true strain of $\varepsilon = 2.3$ and annealed *in-situ* in four steps of increasing temperatures from 170 °C to 560 °C was studied. An increase in the subgrain size and low angle boundary misorientation was accompanied by a halving of the dislocation density from 1.2×10^{16} m^{-2} to 0.6×10^{16} m^{-2}. Limited boundary migration was observed and the increased subgrain size was attributed to the dissolution of dislocations within the low angle boundaries upon annealing.

1. Introduction

When an f.c.c. metal with a high stacking fault energy such as aluminium is deformed to moderate to large strains, energy is stored mostly in dislocation networks in cell walls and within the cells [1]. Upon annealing recovery may occur, leading to the rearrangement of the dislocation networks into sub-boundaries and eventually into a fully developed subgrain structure [2]. For a subgrain to become a viable recrystallization nucleus it needs a size advantage and a high local misorientation to its surroundings [3]. The main mechanisms of nucleation of recrystallization are thought to involve growth of subgrains by low angle boundary migration in an orientation gradient or strain induced boundary migration (SIBM) of existing boundaries. However, the dislocation recovery often required before boundary migration can occur is complex and not very well understood and a full experimental investigation requires a three-dimensional *in-situ* technique able to resolve dislocations [4].

With the developments of automated crystal orientation mapping in the transmission electron microscope (TEM) [5] and calculation of geometrically necessary dislocation (GND) densities from orientation differences in neighbouring map points [6], details of the deformation structure in highly deformed materials can be characterised [7]. In the present work we combine this characterisation with *in-situ* annealing. The objective is to provide measurements of the dislocation recovery and the mechanisms of low angle boundary (LAB) formation and migration in deformed Al, useful for development of recovery and recrystallization models.

2. Experimental

The investigated material was commercial purity Al with a composition of 0.5wt.%Fe and 0.15wt.%Si. The material was direct chill cast and a sample from the billet's centre region was homogenised at 450-600 °C for 120 h and water quenched. The sample had an initial grain size of 58 µm and was cold rolled to a true strain of $\varepsilon = 2.3$.

The hardness and average subgrain size of the deformed sample were determined, the former from a Vickers hardness instrument with a 1 kg load. The subgrain size was determined from electron backscatter diffraction (EBSD) maps from the sample's centre region viewed along the transverse direction (TD). Each map covered an area of 100×100 µm^2 with a step size of 0.1 µm, acquired on a Zeiss Ultra 55 scanning electron microscope operated at 20 kV and equipped with a NORDIF UF1100 detector. EBSD patterns were indexed with the EDAX TSL DC 7.3 software.

Thin foils from the centre region viewed along the normal direction, defined by the rolling direction (RD) and transverse direction, were prepared for TEM observations by mechanical grinding and electropolishing in a Struers Tenupol 3 twin jet polishing unit. The unit was operated at 20 V using an electrolyte of parts 1:2 nitric acid:methanol kept at −30 °C. A JEOL 2100F TEM operated at 200 kV with a Gatan HHST4004 heating holder was used. Scans of precession electron diffraction (PED) patterns were acquired using the NanoMEGAS ASTAR system to map the dislocation recovery and formation and migration of LABs during annealing. In the experiment presented here, a thin foil was annealed in steps according to the procedure in figure 1. Scans were obtained in between the steps at room temperature to ensure that the foil stayed at eusentric height during acquisition.

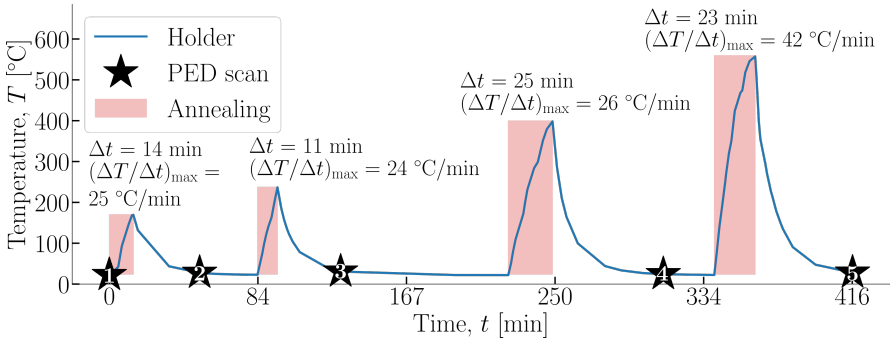

Figure 1. Annealing history for the *in-situ* TEM observation. The annealing interval Δt and max. heating rate $(\Delta T/\Delta t)_{\max}$ for each step and times for PED scans (#1-5) are indicated.

PED patterns were obtained with the microscope operated in nanobeam diffraction mode with a probe convergence semi-angle of 1 mrad and a precession angle of 0.5° and frequency of 100 Hz. A Stingray camera recorded the patterns off of the microscope's fluorescent screen. Five scans of an 8×8 µm^2 region of interest (ROI) with step sizes of 33-40 nm were obtained at times indicated in figure 1. Geometric distortions due to projection optics, shifts of the direct beam and background noise in the patterns were corrected for using the pyXem 0.7 software [8]. NanoMEGAS' template matching was used for pattern indexing.

Orientation data was processed and analysed with the MTEX 5.2 software [9]. Orientations were lightly averaged with the half quadratic filter [10] and grains were reconstructed with a misorientation angle threshold of 0.75° and 0.5° for data from EBSD and PED, respectively. The quality of the orientation averaging and grain reconstruction was assessed by inspection of maps with a quaternion based disorientation colour key [11]. The GND densities were estimated with MTEX based upon work by Pantleon [6]. The $\{111\}\langle 110\rangle$ slip system was assumed active with 12 edge dislocations with line energies $u_{\mathrm{e}} = 1$ and 6 screw dislocations with $u_{\mathrm{s}} = 1-\nu = 1-0.347$, where ν is the Poisson ratio for Al.

3. Results

The deformed sample had a Vickers hardness of 51 and the average subgrain size determined from EBSD was 0.84 µm. Bright field (BF) TEM images of the ROI before annealing and after the final annealing step in figure 2 show that annealing led to the rearrangement of dislocation tangles into boundaries and a more developed subgrain structure. No recrystallization was observed. The numbered (1-3) coloured dots highlight the same areas. Some subgrains disappeared during recovery, like the dark grains of high diffraction contrast below (1) and (3) in (a). Other subgrains developed narrower and more defined boundaries to adjacent subgrains, like the subgrain in (2). Note the development of stable boundary sections with 120° angles near the subgrain highlighted by the arrow in (b).

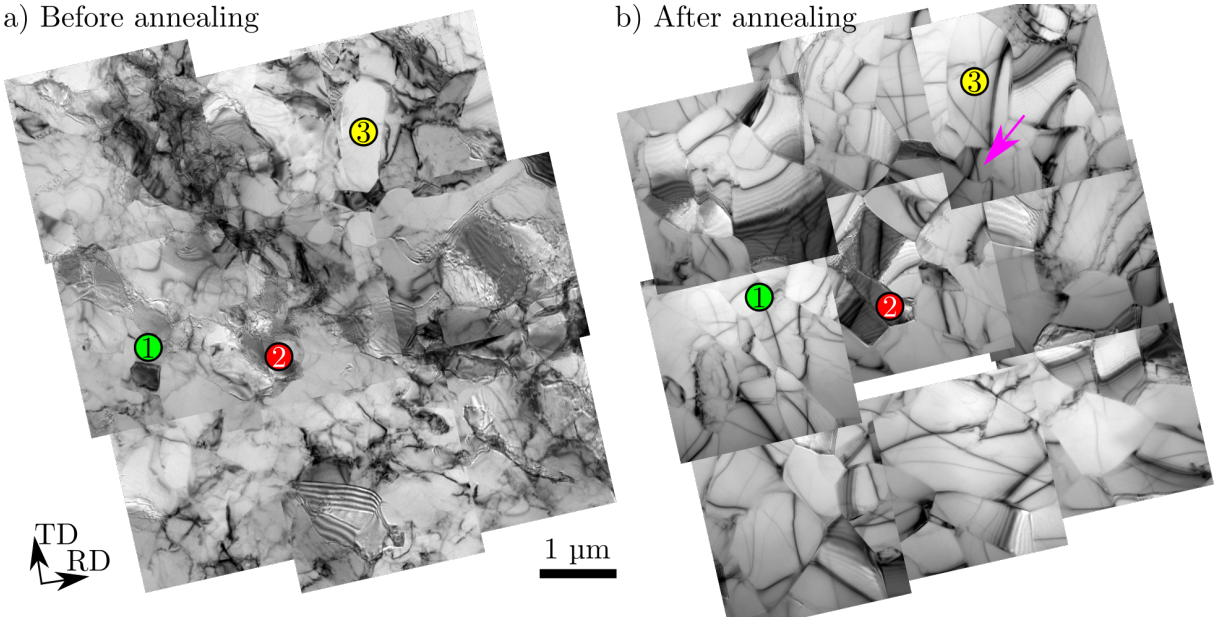

Figure 2. BF TEM images of the ROI (a) before annealing and (b) after the final annealing step. The numbered dots (1-3) indicate the same positions.

Results from the five PED scans are shown in figure 3, with the scale bar in (a) applying to all maps. The correlation index maps indicate the degree of correlation between experimental and simulated diffraction patterns from template matching, with higher correlation in brighter regions. The grain boundary (GB) and disorientation colouring maps show LABs and high angle boundaries (HABs) with misorientations $0.5° < \theta < 15°$ and $> 15°$, respectively. The average grain orientation is grey and deviations from this orientation follow the disorientation colour key as shown in the map in (a). This representation reveals multiple cells or subgrains with boundaries of misorientations below 0.5° that were not reconstructed, clearly demonstrating its usefulness when characterising deformation substructures. The dislocation density maps clearly show the dislocation recovery taking place upon annealing.

Three observations are highlighted in the shapes in figure 3, the first of the subgrain surrounded by the ellipse in (a) with an initial HAB to a large subgrain below and a LAB to its parent grain above. After the 1st annealing step both its boundaries straighten out and the high dislocation density inside appears to be annealed out. However, the dislocation density increases again after the 2nd annealing step and the LAB dissolves after the 3rd annealing step. Simultaneously, while the HAB misorientation stays at 60° the LAB misorientation decreases from 4° before annealing to 1° after the 2nd annealing step and below 1° after the 3rd step.

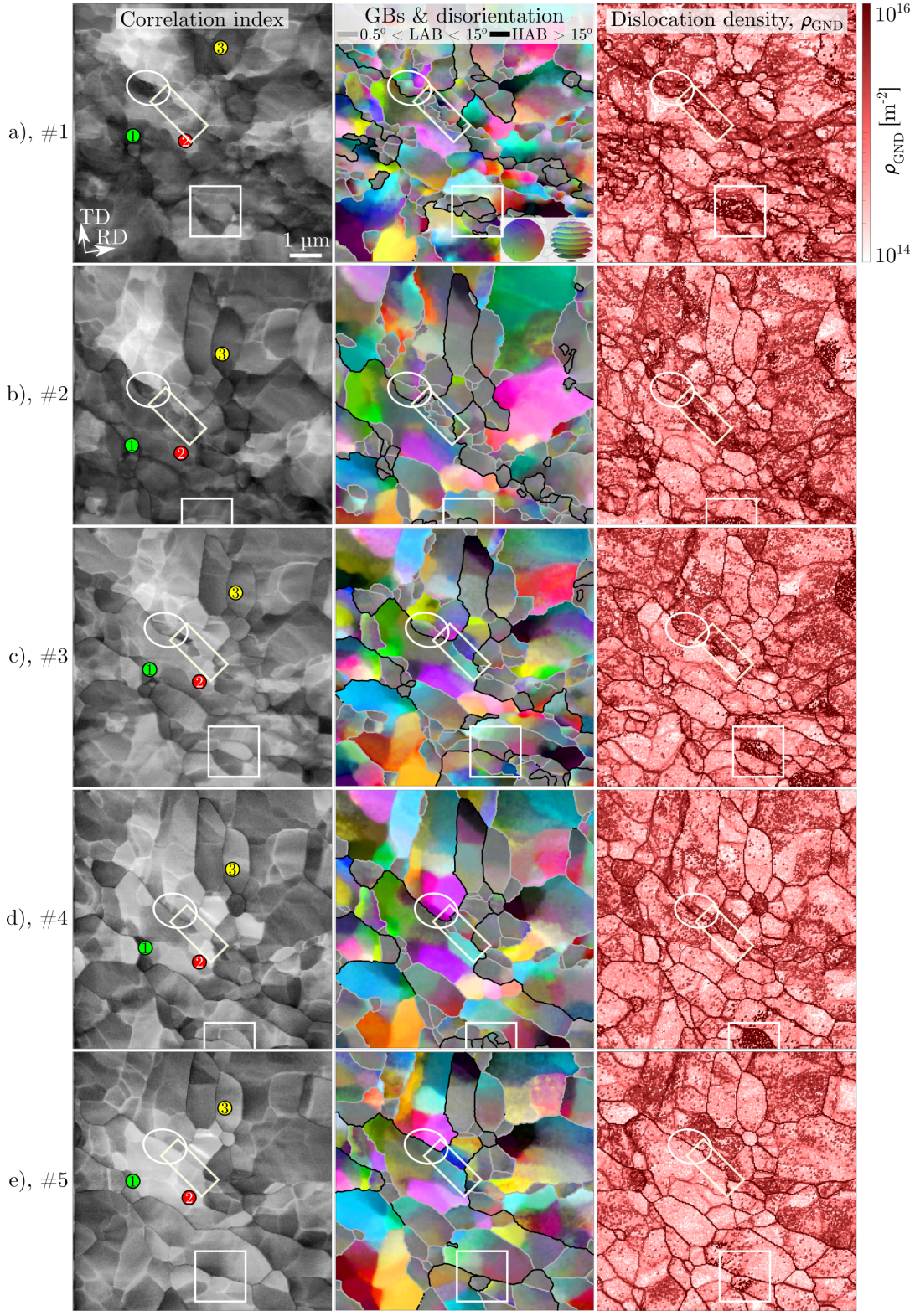

Figure 3. Substructure evolution from the PED scans (#1-5). (Left) Maps of correlation index, (middle) grain boundaries and disorientation colouring and (right) dislocation densities ρ_{GND} (a) before annealing, after (b) the 1st, (c) 2nd and (d) 3rd annealing step and (e) after the final annealing step. See figure 2 and the text for descriptions of dots and shapes, respectively.

After the final step the subgrain is gone and the HAB has moved upwards. Note also in (e) that the parent grain obtains an increased dislocation density during the final step. The second observation is of a group of subgrains surrounded by the rectangle in (a) that upon annealing disappear and leave behind a well defined LAB in (c). The misorientation of this boundary increases at the same time from 6° to 11° after the 2nd annealing step and decreases somewhat to 8° after the final step. The third observation is of a region surrounded by the rectangle in (a) of high dislocation density with a HAB to a subgrain of lower dislocation density above. Upon annealing this region shrinks in size and after the final annealing step it is entirely inside the above subgrain.

The evolution of the average subgrain size δ_{ECD}, given by the equivalent circular diameter (ECD), misorientation θ across LABs and dislocation density ρ_{GND} determined from the PED scans are shown in figure 4 (a-c), respectively. The change in misorientation with subgrain size is shown in (d), with a linear fit with a slope of 10. The subgrain size was observed to increase from 0.42 µm to 0.62 µm, the LAB misorientation increased from 5.3° to 6.2° and the dislocation density halved from 1.2×10^{16} m^{-2} to 0.6×10^{16} m^{-2}.

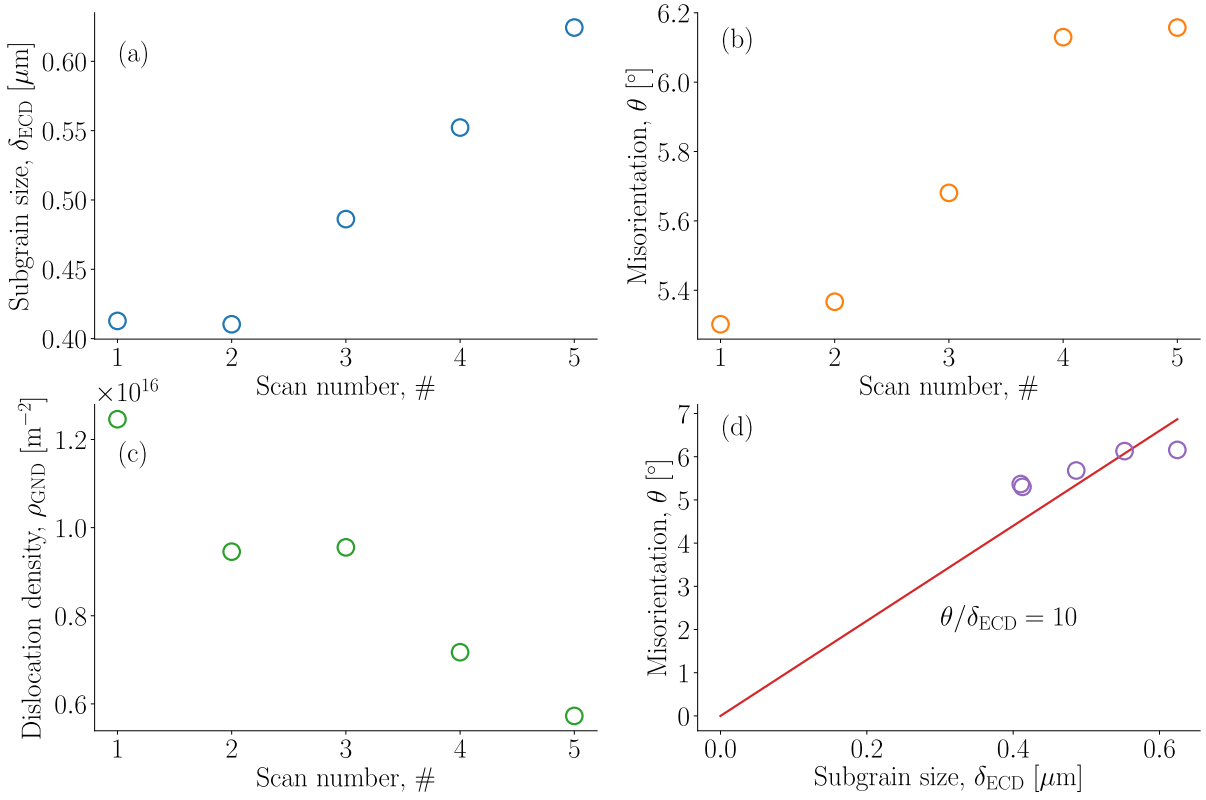

Figure 4. Evolution of substructure parameters from PED scans (#1-5) in figure 3. (a) The average subgrain size δ_{ECD}, (b) LAB misorientation θ, (c) dislocation density ρ_{GND} and (d) change in misorientation with subgrain size.

4. Discussion

Limited LAB migration is observed, and the increased subgrain size in figure 4 (a) is attributed to the dissolution of LABs upon annealing. The first two observations from the PED scans in the ellipse and rectangle in figure 3 indicate such dissolution, as reported in earlier works on a similar alloy by for example Sandström *et al.* [12]. In the first observation, the dislocations

in the LAB appear to have been pulled out by the stress field in the adjacent larger subgrain interior, thus contributing to the increased dislocation density observed in this subgrain after the final annealing step. In the second observation, the dislocations in the LABs appear to have been absorbed by the nearby LAB that experienced an increased misorientation upon annealing. The migration of the HAB in the square in (a) is an example of SIBM, which also seems to be the operating mechanism in the HAB migration in the first observation.

The combination of scanning precession electron diffraction with *in-situ* annealing in the TEM provides details of the dislocation recovery and substructure of metals deformed to large strains not readily available from EBSD in the SEM, exemplified by the results presented here. However, care must be taken when comparing results from thin foils to results from bulk since microstructures experience slower growth upon annealing in thin foils. When performing recrystallization experiments the foil thickness must be chosen according to the amount of stored energy and the size of the substructure. Also, increased resolution leads in this case to reduced statistics. For example, the ROI in this experiment, chosen for its multiple HABs and thus an increased possibility for boundary migration to occur, most likely has a higher dislocation density than the sample overall. The observed dislocation densities $\propto 1 \times 10^{16}\,\mathrm{m}^{-2}$ are much higher than the densities $\propto 1 \times 10^{13}\,\mathrm{m}^{-2}$ reported previously for a similar alloy [13]. These aspects will be considered in future work expanding upon the presented methodology.

5. Conclusions

A commercial purity Al alloy cold rolled to a true strain of $\varepsilon = 2.3$ was *in-situ* annealed in steps in the TEM. Scans of precession electron diffraction patterns were collected to characterise the dislocation recovery and formation of LABs upon annealing. An increase in the subgrain size and LAB misorientation was accompanied by a halving of the dislocation density from $1.2 \times 10^{16}\,\mathrm{m}^{-2}$ to $0.6 \times 10^{16}\,\mathrm{m}^{-2}$. Limited LAB migration was observed and the increased subgrain size was attributed to the dissolution of LABs upon annealing.

Acknowledgments

The authors would like to thank Hydro Aluminium Sunndalsøra for providing the material. HWÅ acknowledges NTNU for financial support through the NTNU Aluminium Product Innovation Centre (NAPIC). The Research Council of Norway is acknowledged for the support of the Norwegian Centre for Transmission Electron Microscopy (NORTEM, Grant No. 197405).

References

[1] Humphreys F J, Rohrer G S and Rollett A D 2017 *Recrystallization and Related Annealing Phenomena* 3rd ed (Oxford: Elsevier)
[2] Nes E 1995 *Acta Metallurgica Et Materialia* **43** 2189–2207
[3] Doherty R D, Hughes D A, Humphreys F J, Jonas J J, Jensen D J, Kassner M E, King W E, McNelley T R, McQueen H J and Rollett A D 1997 *Materials Science and Engineering: A* **238** 219–274
[4] Humphreys F J 2004 *Materials Science Forum* **467** 107–116
[5] Rauch E F, Portillo J, Nicolopoulos S, Bultreys D, Rouvimov S and Moeck P 2010 *Zeitschrift fur Kristallographie* **225** 103–109
[6] Pantleon W 2008 *Scripta Materialia* **58** 994–997
[7] Ghamarian I, Liu Y, Samimi P and Collins P C 2014 *Acta Materialia* **79** 203–215
[8] pyXem developers 2019 pyXem v0.7 `https://github.com/pyxem/pyxem`
[9] Bachmann F, Hielscher R and Schaeben H 2010 *Solid State Phenomena* **160** 63–68
[10] Hielscher R, Silbermann C and Schmidl E 2018 *J. Appl. Crystallogr.-In Rev.*
[11] Thomsen K, Mehnert K, Trimby P W and Gholinia A 2017 *Ultramicroscopy* **182** 62–67
[12] Sandström R, Lehtinen B, Hedman E, Groza I and Karlsson S 1978 *Journal of Materials Science* **13** 1229–1242
[13] Nord-Varhaug K, Forbord B, Benestad J, Pettersen T, Rønning B, Bardal A, Benum S, Marthinsen K and Nes E 2000 *Materials Science Forum* **331** 1387–1392